Odd-parity $J=11/2$ autoionizing Rydberg series of europium below the $5d\ ^9D_4$ threshold: Spectroscopy and multichannel quantum-defect-theory analysis

S. Bhattacharyya,[1] M. A. N. Razvi,[1] S. Cohen,[2] and S. G. Nakhate[1,*]
[1]*Spectroscopy Division, Bhabha Atomic Research Centre, Mumbai 400085, India*
[2]*Atomic & Molecular Physics Laboratory, Physics Department, University of Ioannina, GR-45110 Ioannina, Greece*
(Received 26 March 2007; published 10 July 2007)

The odd-parity $J=11/2$ autoionizing states of europium atom below the $5d\ ^9D_4$ threshold are investigated by a two-step laser photoionization scheme via the $4f^7 5d6p\ ^{10}F_{9/2}$ intermediate state. The observed resonances are classified into two autoionizing Rydberg series (with $n=15$ to 55) converging to the $5d\ ^9D_4$ limit and eight members ($n=13$ to 20) of two autoionizing Rydberg series converging to the higher $5d\ ^9D_5$ limit. The single series converging to the $5d\ ^9D_3$ limit is not efficiently excited. The observed four Rydberg series are assigned in jj coupling as $5dnd\ (4,j)$ and $5dnd\ (5,j)$ with $j=3/2$ and $5/2$. Apart from the $5dnd\ (5,5/2)$ series, the majority of autoionizing resonances exhibits narrow linewidths and quasisymmetric line shapes, reflecting this way the weak coupling between the discrete levels and the adjacent continua. The experimental data are analyzed through the semiempirical phase-shifted multichannel quantum defect theory. The theoretically calculated energy level positions and excitation profiles are in good agreement with the experimental ones, thus confirming the identification of the observed structures. The constructed Lu-Fano plot and computed admixture coefficients reveal weak and localized interactions among the Rydberg series members.

DOI: 10.1103/PhysRevA.76.012502 PACS number(s): 32.30.−r, 32.80.Rm, 32.80.Dz, 31.15.Ct

I. INTRODUCTION

Multichannel quantum defect theory (MQDT) is a powerful tool for describing complex atomic spectra both in the bound and autoionizing spectral range with a limited number of parameters related to quantum defects, interseries interactions and dipole moments. The main field of MQDT application on atomic systems concerns the closed shell alkaline-earth-metal atoms and inert gasses. Open shell atoms (in particular Carbon group atoms, halogens, and open *d*-shell transition metals) have also been treated by combining MQDT with the *R*-matrix technique [1]. However the theory has not been extensively tested in the even more complex lanthanide group of atoms such as europium. The interest in studying this latter atom comes from the fact that while it presents a half-filled $4f$ subshell, it is nevertheless an experimentally convenient two-electron system among lanthanides. Two-electron atomic systems are of constant experimental and theoretical interest because of their apparent resemblance to helium, the prototype atomic three-body Coulomb system. Helium is seemingly the simplest atom to study from the theoretical point of view but it is rather difficult to deal with experimentally due to its high ionization threshold. Alkaline-earth-metal atoms with closed-shell ionic cores present a convenient alternative and have been extensively studied experimentally and theoretically whilst the lanthanides have got the least attention because of their complexity induced by their aforementioned $4f$ open subshell. The coupling of the $4f$ electrons with the two outermost ones gives rise to multiple and closely spaced ionic limits with high angular momentum, which in turn gives rise to many parallel running and interacting Rydberg series converging to these limits. For example, the five $5d\ ^9D_J$ ($J=2-6$) limits, just above the first ionization potential, span an energy range of $\sim 1250\ \mathrm{cm}^{-1}$ while the distance between successive thresholds lies in the range of $\sim 400-200\ \mathrm{cm}^{-1}$. That energy range is largely unexplored and therefore extensive experimental as well as theoretical efforts to reveal configuration interaction and spin-orbit induced interseries mixing effects are of great importance.

Among lanthanides, only the ytterbium spectrum has been previously interpreted with semiempirical eigenchannel MQDT by Aymar *et al.* [2]. In a recent paper [3], we have used the same MQDT variant for analyzing the $J=3/2$ autoionizing Rydberg series of europium up to $^9D_4$ threshold. Nevertheless, the eigenchannel MQDT formulation requires *a priori* knowledge of each channel's configuration and symmetry in order to build the $U_{i\bar{\alpha}}$ unitary matrix connecting the collision channels $\{i\}$ to close-coupling channels $\{\bar{\alpha}\}$. When however, a number of the Rydberg series expected upon symmetry considerations are not efficiently excited or detected, the application of semiempirical eigenchannel MQDT becomes difficult. In such cases more flexibility is offered by the so-called phase-shifted MQDT, introduced by Giusti-Suzor and Fano [4] for the two closed (i.e., bound) channel problem and further developed for a higher number of open and closed channels by Cooke and Cromer [5], Lecomte [6], Ueda [7], Giusti-Suzor and Lefebvre-Brion [8], and Cohen [9].

In the present work, we report experimental data on the $J=11/2$ autoionizing spectrum below the $5d\ ^9D_4$ threshold where the experimentally recorded Rydberg series are indeed less than the expected ones. The data are analyzed with appropriate semiempirical phase-shifted MQDT models and, despite the aforementioned difficulties, it is found possible to successfully reproduce energy levels positions and excitation cross sections. Moreover, channel admixture coefficients among the observed Rydberg series are obtained. The achieved level classification will certainly be of great help to

*Corresponding author. Email address nakhate@barc.gov.in

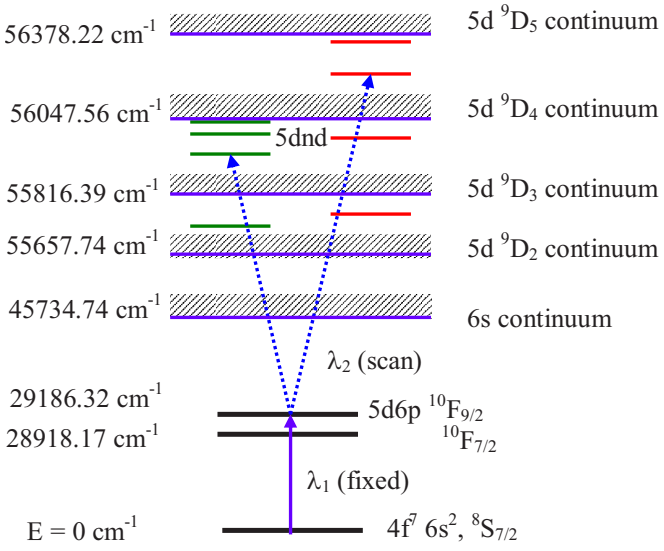

FIG. 1. (Color online) Schematic diagram of the two-step laser photoionization scheme employed for the study of $5dnd$ autoionizing energy levels below the $5d\ ^9D_4$ threshold of europium atom.

the preparation of further spectroscopic and theoretical studies on europium atom.

II. EXPERIMENTAL DETAILS

The experimental technique was described in detail in our previous paper [10]. Briefly, the autoionizing Rydberg levels below the $^9D_4$ threshold are accessed via a two step resonance photoionization scheme. The laser system consists of two pulsed dye lasers of line width 0.2 cm^{-1} and pulse duration 25 ns pumped by a XeCl excimer laser. Europium vapor is generated in a crossed heat-pipe oven operated at 800 K. The resulting europium vapor pressure is around 0.2 mbar. The excitation scheme for approaching autoionization resonances in the spectra of europium is shown in Fig. 1. The atoms are excited by the first dye laser using the dye *p*-terphenyl to the $4f^7 5d(^9D)6p\ ^{10}F_{7/2,9/2}$ intermediate levels located at 28 918.17 and 29 186.32 cm^{-1}, respectively. The second dye laser is scanned to probe the autoionizing resonances in the energy range 55 280–56 050 cm^{-1} using the dye Butyl-PBD. The pulse energy of the dye lasers is about 0.5 mJ and their beam diameter in the interaction region is ~5 mm. The dye laser beams are aligned to have optimum spatial and temporal overlap in the interaction region. The second dye laser is delayed by ~12 ns with respect to the first dye laser in order to avoid effects such as ac stark shifts and multiphoton absorptions. The photoions generated in the process of autoionization were detected by a hot cathode thermionic diode, mounted inside the heat pipe oven and operated in the space charge limited region. For wavelength calibration, a small fraction of the scanning dye laser beam passes through a Uranium-Neon hollow cathode lamp and another fraction to a photodiode through a 1.364 cm^{-1} free spectral range Fabry-Pérot etalon. The standard optogalvanic lines of uranium and etalon fringes are used to calibrate the europium spectra. All the signals are processed by independent channels of a boxcar integrator, recorded simultaneously as a function of wavelength, and stored on a personal computer.

III. RESULTS AND DISCUSSION

A. Preliminary assignments

The total angular momentum quantum number J for each observed final level is derived by a comparison between the spectra recorded from the two $5d6p\ ^{10}F_J$ intermediate levels with $J=9/2$ and $7/2$ and the application of the single photon dipole selection rules ($\Delta J=0,\pm 1$ but $0\leftrightarrow 0$ forbidden). Thus $J=11/2$ final states may be reached only by the $J=9/2$ intermediate level while they are not excited from the $J=7/2$ one. The experimental energies, reported in Table I, refer to the line maxima since the majority of $J=11/2$ resonances exhibit quasisymmetric line profiles. Their ~0.5 cm^{-1} estimated uncertainty is dictated mainly by the laser linewidth and data acquisition rate.

For each particular level of energy E the effective quantum numbers υ_j corresponding to every relevant ionic limit E_{Dj} ($j=3$, 4, 5, and 6) are calculated using $\nu_j=[\mathrm{Ry_{Eu}}/(E_{Dj}-E)]^{1/2}$, with $\mathrm{Ry_{Eu}}=109\,736.918\ cm^{-1}$, the europium mass corrected Rydberg constant. A preliminary level assignment is obtained by grouping the levels having the same effective quantum number fractional parts (with respect to the same limit). Of additional help are the comparable line intensities and line shapes exhibited by members belonging to a particular Rydberg series. Further classification refinement is accomplished by constructing a number of $(\nu_j,\nu_{j'})$ Lu-Fano plots, i.e., by projecting the same experimental data to different ν_j planes. This procedure revealed two autoionizing Rydberg series converging to $5d\ ^9D_4$, eight members of two series converging to the higher $5d\ ^9D_5$ limit and a small number of unclassified $J=11/2$ resonances. At this point it is useful to consider all the $J=11/2$ Rydberg series which are accessible through the $5d6p\ ^{10}F_{9/2}$ intermediate level and build on the ^9D_J limits. These are the following:

$$
\begin{aligned}
5d6p\,^{10}F_{9/2} &\rightarrow 5dnd(3,5/2)_{11/2}\\
&\rightarrow 5dnd(4,j)_{11/2} \text{ with } j=3/2 \text{ and } 5/2\\
&\rightarrow 5dnd(5,j)_{11/2} \text{ with } j=3/2 \text{ and } 5/2\\
&\rightarrow 5dns(5,1/2)_{11/2}\\
&\rightarrow 5dnd(6,j)_{11/2} \text{ with } j=3/2 \text{ and } 5/2\\
&\rightarrow 5dns(6,1/2)_{11/2}.
\end{aligned}
$$

The *jj*-coupling scheme is adopted here since europium is a high-Z atom, the reported levels possess high principal quantum numbers n ($n\geqslant 13$) and it is moreover noticed that the observed Rydberg series are more or less grouped into pairs with splittings scaling as υ^{-3}. To the above series one has to add the $4f^7 6s(^9S_4)\varepsilon d_{5/2,3/2}$ ($^{10}D_{11/2}$ and $^8D_{11/2}$ in LS notation) and $4f^7 6s(^7S_3)\varepsilon d_{5/2}$ ($^8D_{11/2}$) continua. It would be interesting to discuss the fact that from the nine expected series (seven of $5dnd$ configuration and two of $5dns$ configuration) only four are experimentally observed. Since there are no $5dns$ series associated with the $5d\ ^9D_4$ limit the observed two

TABLE I. Experimental and theoretical energies and assignments of $J=11/2$ autoionizing series below $5d\,^9D_4$ threshold. $d--$, $d-+$, $d+-$, and $d++$ stands for $5dnd$ $(4,3/2)$, $5dnd$ $(4,5/2)$, $5dnd$ $(5,3/2)$, and $5dnd$ $(5,5/2)$ configuration, respectively, where n is the principal quantum number. The experimentally unresolved pair of members of the two series $5dnd$ $(4,j)$ with $j=3/2$ and $5/2$ of a given n is listed as nd. Admixture coefficients larger than 10% in a channel are given in brackets.

Assignment	E_{expt} (cm^{-1})	E_{theor} (cm^{-1})	$E_{\text{expt}}-E_{\text{theor}}$	Admixture coefficients in other channels
15$d--$ [78]	55 312.4	55 312.4	0.0	$d+-$ [14]
15$d-+$ [81]	55 315.4	55 317.3	−1.9	$d--$ [13]
13$d+-$ [82]	55 329.5	55 328.9	0.6	$d-+$ [10]
13$d++$ [98]	55 368.7	55 367.7	1.0	
16$d--$ [100]	55 421.0	55 421.0	0.0	
16$d-+$ [96]	55 424.0	55 424.6	−0.6	
17$d--$ [65]	55 504.3	55 504.0	0.3	$d+-$, $d-+$ [25, 10]
17$d-+$ [68]	55 508.1	55 507.5	0.6	$d--$ [26]
14$d+-$ [69]	55 512.9	55 513.3	−0.4	$d-+$, $d--$ [20, 11]
14$d++$ [97]	55 541.7	55 541.8	−0.1	
18$d--$ [100]	55 575.0	55 574.7	0.3	
18$d-+$ [99]		55 576.9		
"P"	55 580.1			
19$d--$ [97]	55 630.0	55 630.9	−0.9	
19$d-+$ [95]	55 632.4	55 632.6	−0.2	
15$d+-$ [95]	55 650.6	55 648.9	1.7	
15$d++$ [94]	55 669.5	55 668.2	1.3	
"P"	55 676.4			
20$d--$ [99]	55 679.4	55 678.2	1.2	
20$d-+$ [91]	55 681.1	55 680.1	1.0	
21$d--$ [44]	55 717.3	55 717.6	−0.3	$d++$ [54]
21$d-+$ [100]	55 718.6	55 718.7	−0.1	
22$d--$ [68]	55 750.0	55 750.1	−0.1	$d-+$, $d+-$ [16, 12]
22$d-+$ [85]		55 751.8		
"P"	55 754.0			
16$d+-$ [84]	55 756.4	55 755.9	0.5	
16$d++$ [96]	55 767.0	55 767.1	−0.1	
23$d--$ [99]	55 779.5	55 779.6	−0.1	
23$d-+$ [90]	55 780.7	55 780.8	−0.1	
24$d--$ [95]	55 804.3	55 804.2	0.1	
24$d-+$ [55]	55 805.7	55 805.1	0.6	$d++$ [45]
25d [92]	55 826.2	55 825.8	0.4	
17$d+-$ [54]	55 840.9	55 841.2	−0.3	$d++$ [44]
26d [82]	55 844.4	55 845.1	−0.7	
27d [96]	55 861.4	55 861.4	0.0	
28d [96]	55 875.5	55 875.7	−0.2	
29d [92]	55 888.2	55 888.4	−0.2	
30d [99]	55 899.4	55 899.9	−0.5	
18$d+-$ [55]	55 908.1	55 908.9	−0.8	$d++$ [35]
31d [82]	55 909.3	55 910.0	−0.7	
32d [96]	55 919.4	55 919.6	−0.2	
33d [100]	55 927.7	55 927.8	−0.1	
34d [90]	55 935.2	55 935.4	−0.2	
35d [53]	55 942.0	55 942.2	−0.2	$d++$ [47]

TABLE I. (*Continued.*)

Assignment	E_{expt} (cm^{-1})	E_{theor} (cm^{-1})	$E_{\text{expt}}-E_{\text{theor}}$	Admixture coefficients in other channels
36*d* [96]	55 948.1	55 948.4	−0.3	
37*d* [96]	55 953.9	55 954.1	−0.2	
38*d* [97]	55 959.1	55 959.2	−0.1	
39*d* [92]	55 964.0	55 964.1	−0.1	
19*d*++ [40]	55 964.0	55 965.5	−1.5	*d*+−, *d* [27, 33]
40*d* [97]	55 968.7	55 968.6	0.1	
41*d* [98]	55 972.5	55 972.7	−0.2	
42*d* [94]	55 976.3	55 976.5	−0.2	
43*d* [100]	55 979.7	55 979.9	−0.2	
44*d* [99]	55 982.9	55 983.1	−0.2	
45*d* [99]	55 986.1	55 986.1	0.0	
46*d* [95]	55 988.8	55 988.9	−0.1	
47*d* [92]	55 991.6	55 991.5	0.1	
20*d*++ [100]	55 994.1	55 994.0	0.1	
49*d* [91]	55 996.1	55 996.3	−0.2	
50*d* [95]	55 998.3	55 998.4	−0.1	
51*d* [100]	56 000.3	56 000.4	−0.1	
52*d* [100]	56 002.1	56 002.3	−0.2	
53*d* [99]	56 004.3	56 004.1	0.2	
54*d* [99]	56 005.8	56 005.8	0.0	
55*d* [97]	56 007.4	56 007.4	0.0	

series converging to that limit are certainly of 5*dnd* configuration. Taking into account the $\upsilon=1.65$ effective quantum number of the low-lying $4f^7 5d(^9D)6s\ ^8D_{11/2}$ level at 16 079.76 cm^{-1} listed in NBS tables [11] and the fact that the υ[modulo 1] values of all recorded series with respect to the $5d\ ^9D$ limits are in the range 0.2–0.4 we may rule out observation of the 5*dns* $(5,1/2)_{11/2}$ series. Hence the two series converging to the $^9D_5$ threshold are of 5*dnd* configuration as well.

It is remarkable that only a few very weak and diffuse 5*dnd* $(3,5/2)_{11/2}$ series members are recorded below the $5d\ ^9D_3$ threshold. Their excitation is comparable in strength to the continuum excitation and due to their small number they are of limited usefulness in probing interseries interactions and we do not report them here. The weakness of their excitation, however, is not to be attributed solely to a low radiative coupling with the $5d6p\ ^{10}F_{9/2}$ intermediate level, because we do observe an increased background signal when the second dye laser frequency is scanned across the $5d\ ^9D_3$ limit (onset of ionization). We anticipate therefore that the disappearance of that series is also connected to an appreciable coupling to the available continua and subsequently to large autoionization widths. It may be speculated that similar arguments hold for the unobserved $(6,j)_{11/2}$ $j=3/2,5,2$ series while the absence of 5*dns* levels can be rather easily explained by the fact that these series are of exactly the same symmetry with the $6s\varepsilon d$ continua to which they are allowed to autoionize by configuration interaction. The above discussion is also supported by the fact that the four efficiently excited series exhibit narrow linewidths [of the order of 1 cm^{-1} (full width at half maximum) or less], implying a coupling to the continua which is not favored by symmetry considerations. The only exception concerns the $(5,5/2)_{11/2}$ series which shows somewhat larger autoionization widths below the $5d\ ^9D_3$ threshold and a sudden decrease of oscillator strength above it. The latter effect reflects the additional broadening caused by its coupling and subsequent autoionization to the $5d\varepsilon d$ (3,5/2) continuum. Note however that this coupling is of different origin because it is spin-orbit induced and not caused by configuration interaction.

Before concluding this first attempt to analyze the experimental data let us note that there are three resonances that can not be classified to any of the $4f^7 5d\ (^9D_J)nd,s$ series. Their effective quantum numbers calculated with respect to $5d\ ^9D_3$ and $5d\ ^9D_6$ limits are 21.55, 27.99, and 41.92 and 9.25, 9.62, and 9.95, respectively while, as mentioned above, the fractional part of effective quantum numbers of the observed 5*dnd* series falls in the 0.20–0.40 range. To rule out a possible 6*pnp* series excitation (that may also be achieved via the $5d6p\ ^{10}F_{9/2}$ intermediate level) we note that there are two $4f^7(^8S_{7/2})\ 6p^2\ (^1D_2)\ ^8D$ and $4f^7(^8S_{7/2})\ 6p^2\ (^3P_2)\ ^{10}P$ low-lying $J=11/2$ levels. The ^{10}P term is listed in the NBS table at 41 443.70 cm^{-1} while the ^8D term was located close to the first ionization potential (45 734.74 cm^{-1}) by Nakhate *et al.* [12]. By extrapolation it is found that the $6p7p$ configuration based levels should lie above 57 200 cm^{-1}, i.e., well beyond the investigated energy range. On the other hand, the effective quantum numbers for these three reso-

nances, calculated with respect to the fine-structure averaged $4f^7 5d$ (^7D) limit (3.89, 3.91, and 3.93), are in good agreement with the ν[modulo 1] values of the three bound $4f^7 5d^2$ (unassigned levels) [11] at 32 480.95, 35 204.58, and 35 460.74 cm^{-1} which are 1.90, 1.99, and 2.00, respectively. The extra $J=11/2$ resonances may thus be low members of $4f^7 5d(^7D)nl$ series. However a more rigorous identification requires higher energy experimental data and their assignment is a matter of speculation at present. Therefore, while they are listed in Table I, they are not considered in the following MQDT analysis and they are collectively labeled as "*P*" (perturbers) in the column of computed admixture coefficients.

B. MQDT analysis below the $5d\,^9D_3$ threshold

Below the $5d\,^9D_3$ limit the $5dnd$ (4, j), $j=3/2,5/2$ series members are experimentally resolved from $n=15$ to 24, while those converging to the higher $^9D_5$ limit are resolved from $n=13$ to 16. Principal quantum numbers are assigned by referring to the lowest bound $5d^2$ states [11]. It is our purpose here to analyze parametrically energy level positions, channel admixture coefficients and lineshapes through the phase-shifted reaction matrix MQDT formalism. A systematic study of autoionization widths is not possible because for most lines they are of the order of our laser linewidth.

For a general MQDT model, the basic matrix equation to be solved is

$$[\mathbf{R}' + \mathbf{T}]\mathbf{a} = 0, \tag{1}$$

where $\mathbf{R}'$ is the phase-shifted reaction matrix whose diagonal elements are zero and the off-diagonal elements represent interchannel couplings. $\mathbf{T}$ is a diagonal matrix whose elements are given by $T_i=\tan[\pi(\nu_i+\mu_i)]$, where ν_i are the effective quantum numbers and the parameters μ_i may be interpreted as the zero-coupling quantum defects of each channel, i.e., when $\mathbf{R}'=\mathbf{0}$. The $\mathbf{a}$ vector is related to the channel admixture coefficient vector $\mathbf{Z}$ as $a_i=Z_i\cos[\pi(\nu_i+\mu_i)]$. The compatibility equation for Eq. (1) to have a nontrivial solution reads

$$\det[\mathbf{R}' + \mathbf{T}] = 0. \tag{2}$$

Our strategy is to proceed in two steps. In the first, the open channels (continua) are discarded and we consider only the closed channels system (bound states). By fitting solely energy level positions the parameters relevant to this system are first determined. Then, in a second step the open channels are added, allowing the fitting of excitation cross sections. For the sharp resonances of the problem at hand this procedure has the advantage of a minimal readjustment of the parameters pertaining to the closed channel system during the second step. The latter is composed by the $5dnd$ (4,3/2) (channel 1) and $5dnd$ (4,5/2) (channel 2) series both converging to the $5d(^9D_4)$ limit and the $5dnd$ (5,3/2) (channel 3) and $5dnd$ (5,5/2) (channel 4) series converging to the $5d(^9D_5)$ limit. The $5dnd$ (3,5/2) closed channel is neglected because of the lack of reliable data and because its weak spectral appearance allows one to treat it as a quasicontinuum. We are aware that by doing that the spin-orbit induced interaction of this channel with the (5,5/2) series mentioned in the previous subsection is not explicitly taken into account. This coupling may nevertheless be described implicitly by the introduction of energy dependent parameters [13]. Furthermore, zero coupling is assumed between Rydberg series converging to the same limit. This assumption implies a rotation of the original channels so the channel labels are, strictly speaking, only tentative. Nevertheless, the trend of energy levels and finally obtained admixture coefficients shows that in our case they are fairly meaningful.

The compatibility equation (2) for the closed channels system is written as

$$\begin{vmatrix} \tan[\pi(\nu_{D4}+\mu_1)] & 0 & R'_{13} & R'_{14} \\ 0 & \tan[\pi(\nu_{D4}+\mu_2)] & R'_{23} & R'_{24} \\ R'_{13} & R'_{23} & \tan[\pi(\nu_{D5}+\mu_3)] & 0 \\ R'_{14} & R'_{24} & 0 & \tan[\pi(\nu_{D5}+\mu_4)] \end{vmatrix} = 0 \tag{3}$$

and theoretical line positions are obtained by the simultaneous satisfaction of Eq. (3) and the relation between υ_{D4} and υ_{D5}

$$E = E_{D4} - \frac{\mathrm{Ry_{Eu}}}{\nu_{D4}^2} = E_{D5} - \frac{\mathrm{Ry_{Eu}}}{\nu_{D5}^2}. \tag{4}$$

The fitted parameters at this stage are the μ_i's ($i=1-4$) and R'_{13}, R'_{14}, R'_{23} and R'_{24} (with an ambiguity concerning their sign). As expected, for μ_3 and μ_4, it was found necessary to adopt quadratic energy dependence, namely

$$\mu_i = \mu_i^0 + \mu_i^1(\Delta E) + \mu_i^2(\Delta E)^2 \quad i=3,4, \tag{5a}$$

where

$$\Delta E = \frac{(E_{D5}-E)}{\mathrm{Ry_{Eu}}}. \tag{5b}$$

The obtained good quality of the (twelve parameter) fit may be appreciated by its graphical representation, the Lu-Fano plot of Fig. 2, and by the comparison of experimental and fitted energy levels in Table I.

The simulation of the spectrum is accomplished by the introduction of a single open channel (channel 5) representing an effective continuum [6], interpreted as a linear combination of the three true continua built on $6s$ ($^9S_4$) and $6s$ ($^7S_3$) ionic levels. The incorporation of two open channels would be certainly preferable in order to avoid unobserved stabilization effects (quasizero autoionization widths and diverging cross section) [9]. However, augmentation of the MQDT model by a single open channel results to eight additional parameters. The addition of two open channels therefore would render the fitting procedure very difficult. Nevertheless, the fitted parameters do not satisfy the stabilization conditions on the locations of the observed resonances. Besides, the simulated spectra are convoluted with the laser linewidth of 0.2 cm^{-1} and evaluated on an energy mesh equal to that of our data acquisition system. The augmented $[\mathbf{R}'+\mathbf{T}]$ matrix is given by

$$[\mathbf{R}'+\mathbf{T}]=\begin{bmatrix} \tan[\pi(\nu_{D4}+\mu_1)] & 0 & R'_{13} & R'_{14} & R'_{15} \\ 0 & \tan[\pi(\nu_{D4}+\mu_2)] & R'_{23} & R'_{24} & R'_{25} \\ R'_{13} & R'_{23} & \tan[\pi(\nu_{D5}+\mu_3)] & 0 & R'_{35} \\ R'_{14} & R'_{24} & 0 & \tan[\pi(\nu_{D5}+\mu_4)] & R'_{45} \\ R'_{15} & R'_{25} & R'_{35} & R'_{45} & T_5 \end{bmatrix} \tag{6}$$

with $T_5=\tan(-\delta)$ and δ, the energy dependent phase shift of the open channel. For the photoionization cross section σ we adopt the expression of Baig *et al.* [14] which reads

$$\sigma \propto \frac{\left|\sum_1^5 C_{5i}d'_i\right|^2}{C_{55}^2+\left|\sum_1^4 C_{5i}R'_{5i}\right|^2}. \tag{7}$$

The C_{5i} are the cofactors of the fifth row and ith column of the determinant in Eq. (7). The new parameters are the R'_{i5} ($i=1-4$) couplings between closed channels and the continuum and the d'_i ($i=1-5$) transition dipole moments between the initial (intermediate) level and the ith channel. The latter are calculated relatively to the continuum dipole moment, since we are only interested in relative cross sections. Furthermore, for taking into account the $J\neq 11/2$ continuum excitation, a constant background term was incoherently added to σ.

The experimental and simulated spectra are shown in Figs. 3(a) and 3(b) (in mirror-plot form) while the full set of fitted MQDT parameters are given in Table II. The overall agreement in the range 55 300–55 810 cm^{-1} is satisfactory, especially if one considers the overlap of $J\neq 11/2$ resonances [a typical example is the $5d14d$ (5,3/2) line blended with a $J=9/2$ level] and residual perturbations not taken into account by the model. In particular, a comparison of experimental and theoretical results in both the Lu-Fano plot of Fig. 2 and the spectra of Fig. 3 shows the influence of the "P" levels. Specifically, their presence leads to the disappearance of the lines corresponding to the $5d18d$ (4,5/2) and $5d22d$ (4,5/2) levels predicted by MQDT at 55 576.9 cm^{-1} and 55 751.8 cm^{-1}, respectively, and to a $\sim$1 cm^{-1} discrepancy between theory and experiment in the vicinity of the $5d20d$ (4,j) series member. Furthermore, in the neighborhood of "P" levels an irregularity of the relative intensities is clearly observed. Finally, as a general remark, we may note from Table II that the mixing among the fitted Rydberg series as well as their coupling to the continuum is fairly weak.

C. MQDT analysis between the $5d\ ^9D_3$ and $5d\ ^9D_4$ limits

Above the $5d\ ^9D_3$ threshold, the members of the two $5dnd$ (4,j) with $j=3/2,5/2$ series are hardly resolved and gradually merged. They are recorded as unresolved doublets up to $n=55$. The $5dnd$ (5,3/2) series constitutes the main perturbers in this energy range while the $5dnd$ (5,5/2) series

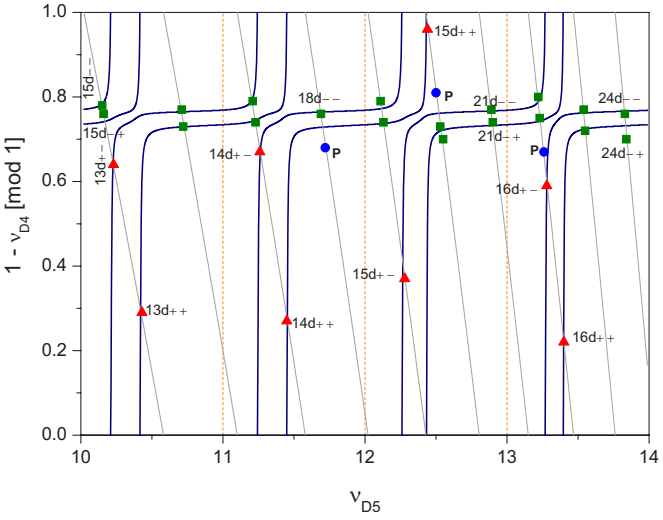

FIG. 2. (Color online) Lu-Fano plot of the $J=11/2$ autoionizing levels of europium in the ν_{D4} (mod 1) versus ν_{D5} plane. The squares represent experimental energy levels and the full curve is calculated with the phase-shifted MQDT parameters involving only closed channels listed in Table II. $d--$, $d-+$, $d+-$, and $d++$ stands for $5dnd$ (4,3/2), $5dnd$ (4,5/2), $5dnd$ (5,3/2) and $5dnd$ (5,5/2) configuration, respectively.

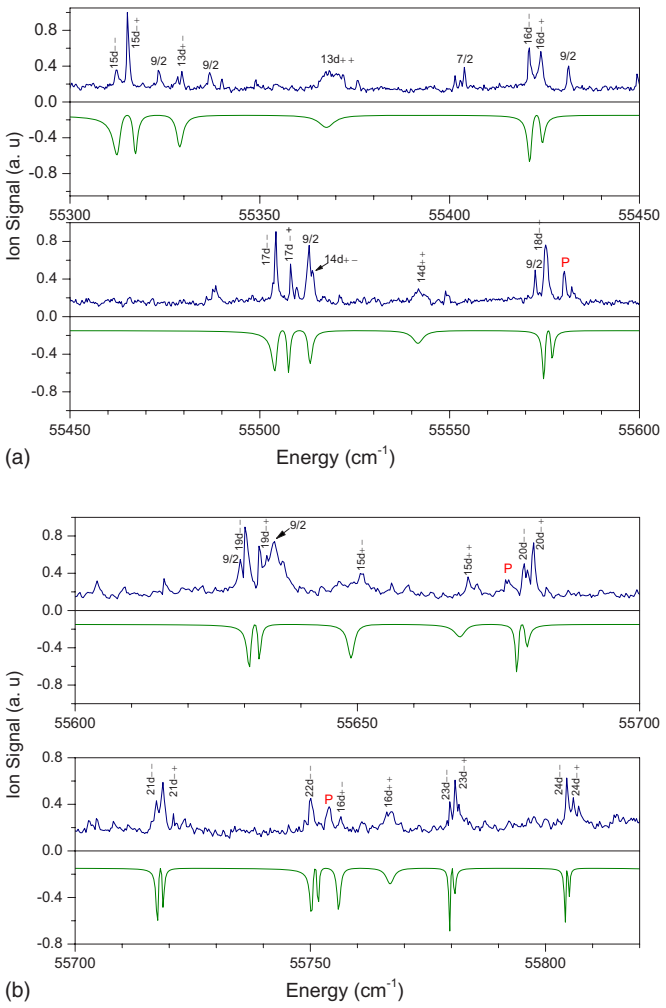

FIG. 3. (Color online) (a). Experimental (top) and simulated (below) spectra in the energy range 55 300–55 600 cm^{-1} given as a mirror plot. (b) Experimental (top) and simulated (below) spectra in the energy range 55 600–55 800 cm^{-1} given as a mirror plot.

members becomes too weak and only occasionally observed. Despite these difficulties and in order to treat the problem below as well as above the $^9D_3$ limit cohesively, we adopted the same closed channel system as that below the $^9D_3$ limit [i.e., two $5dnd$ $(4,j)$ and two $5dnd$ $(5,j)$ series] and added another open channel. A schematic diagram of this six-channel model (6QDT) is shown in Fig. 4. To keep the number of fitted parameters reasonable, the two continua are considered uncoupled and only the $5dnd$ $(5,j)$ series are coupled to the new open channel (while they are uncoupled from the other effective continuum). Based on the discussion of Sec. III A explaining the sudden disappearance of the $5dnd$ $(5,5/2)$ series the new open channel may tentatively assigned to represent the $5d\varepsilon d$ $(3,5/2)$ continuum. One, however, has to keep in mind that the introduction of uncoupled open channels is equivalent to a linear combination of the true continua. The matrix equation and compatibility condition for the two-open channel 6QDT problem are identical in form to Eqs. (1) and (2). The diagonal elements T_5 and T_6 of the two open channels are written in terms of a common phase shift $\delta^{(\rho)}$ such that $T_5=T_6=\tan[\pi(-\delta^{(\rho)})]\equiv\varepsilon_\rho$. By solv-

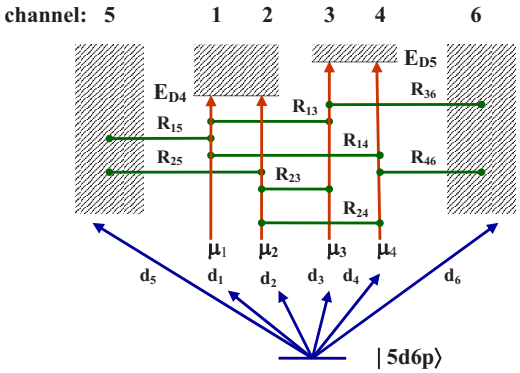

FIG. 4. (Color online) Schematic diagram of the phase-shifted four closed and two open channel phase shifted 6QDT model.

ing Eq. (2) (a quadratic equation in ε_ρ) the two roots of ε_ρ for $\rho=1,2$ are obtained. Equation (1) is then solved together with the normalization condition $(a_5^{(\rho)})^2+(a_6^{(\rho)})^2=(1+\varepsilon_\rho^2)^{-1}$ to determine $a_i^{(\rho)}(i=5,6)$ for $\rho=1$ and 2 for the ith channel. The photoionization cross section of the autoionizing resonances excited from the intermediate state is written as

$$\sigma(E)\propto\sum_{\rho=1}^{n_o}\left[\sum_{i=1}^{N}a_i^{(\rho)}d_i'\right]^2, \tag{8}$$

where $N=6$ is the total number of channels and $n_o=2$ the number of open channels. The photoionization cross section σ is calculated following procedures similar to those described in Sec. III B. Again experimental energy levels are fitted first, providing the closed channel quantum defects μ_i and interchannel interactions R_{ij}' between closed channels. The fitted values below the $^9D_3$ limit served as initial guesses for these parameters and only a small adjustment is found necessary. Furthermore, there is no need to employ energy dependent quantum defects in this energy range. The experimental and calculated energy level positions in this energy range are listed in Table I. During the second step, the ratio

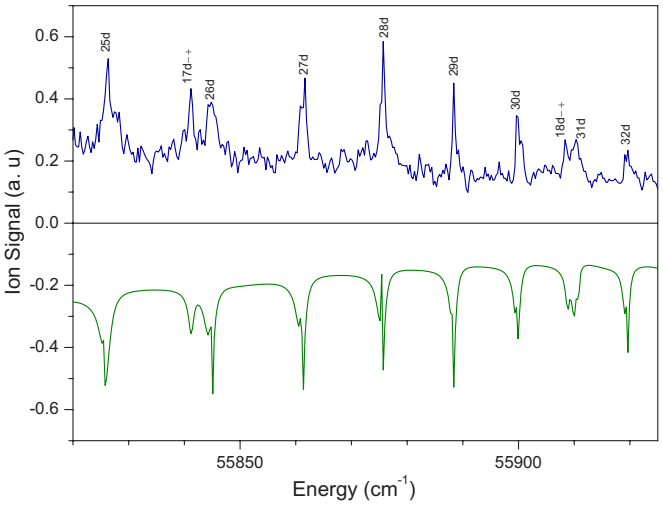

FIG. 5. (Color online) Experimental (top) and simulated (below) spectra between the $5d$ $^9D_3$ and $^9D_4$ thresholds in the energy range 55 800–55 950 cm^{-1} given as a mirror plot.

TABLE II. Phase-shifted MQDT parameters for the analysis of the autoionizing Rydberg series spectra of europium below the $5d\ ^9D_4$ threshold. The Eu mass corrected Rydberg constant is $Ry_{Eu}=109\,736.918\ cm^{-1}$.

Data below the $5d\ ^9D_3$ limit

Channel i	Ionization limit	μ_i	d_i'/d_5'
(1) $5dnd$ (4,3/2)	56 047.56 cm^{-1}	$\mu_1=0.766\ (\pm0.001)$	4.9 (±0.1)
(2) $5dnd$ (4,5/2)		$\mu_2=0.732\ (\pm0.001)$	−3.8 (±0.1)
(3) $5dnd$ (5,3/2)	56 378.22 cm^{-1}	$\mu_3=0.760(\pm0.001)-17.9(\pm0.5)\Delta E+2152(\pm47)\Delta E^2$	3.9 (±0.1)
(4) $5dnd$ (5,5/2)		$\mu_4=1.30(\pm0.01)-198(\pm1)\Delta E+13012(\pm100)\Delta E^2$	3.2 (±0.2)
(5) Effective continuum			1

Phase shifted reaction matrix

	1	2	3	4	5
1	0	0	0.09 (±0.004)	0.06 (±0.01)	0.15 (±0.01)
2		0	0.08 (±0.004)	0.10 (±0.01)	−0.14 (±0.01)
3			0	0	0.14 (±0.01)
4				0	0.19 (±0.02)
5					0

Data between the $5d\ ^9D_3$ and $^9D_4$ limits

Channel i	Ionization limit	μ_i	d_i'/d_5'
(1) $5dnd$ (4,3/2)	56 047.56 cm^{-1}	$\mu_1=0.760\ (\pm0.002)$	2.0 (±0.2)
(2) $5dnd$ (4,5/2)		$\mu_2=0.736\ (\pm0.002)$	−3.5 (±0.1)
(3) $5dnd$ (5,3/2)	56 378.22 cm^{-1}	$\mu_3=0.702\ (\pm0.001)$	1.4 (±0.1)
(4) $5dnd$ (5,5/2)		$\mu_4=0.60\ (\pm0.02)$	1.0 (±0.2)
(5) Effective continuum			1
(6) "$5d\varepsilon d$ (3,5/2)"			−0.70 (±0.4)

Phase shifted reaction matrix

	1	2	3	4	5	6
1	0	0	0.10 (±0.01)	0.06 (±0.02)	0.30 (±0.02)	0
2		0	0.10 (±0.01)	0.10 (±0.02)	−0.3 (±0.02)	0
3			0	0	0	0.18 (±0.03)
4				0	0	0.50 (±0.06)
5					0	0
6						0

of the matrix elements $d_i/d_5(i=1-4,6)$ and closed to open channel interaction parameters R'_{15}, R'_{25}, R'_{36}, and R'_{46} are optimized by fitting the experimental spectrum to Eq. (6) and keeping μ_i and R'_{ij} nearly constant as determined from the Lu-Fano plot. A (quadratic) energy dependent background term is added to σ in order to match the experimentally recorded background excitation. The calculated spectra are convoluted with laser linewidth of 0.2 cm^{-1} and evaluated on an energy mesh equal to that of our data acquisition system. The experimental and the calculated spectra are shown in Fig. 5 and the whole set of phase-shifted MQDT parameters are given in Table II.

The part of experimental and theoretical spectrum in the range 55 820–55 920 cm^{-1} is shown in the mirror plot of Fig. 5. The gradual merging of $5dnd$ $(4,j)$ members (see, for example, the line labeled as $27d$) and the line shapes in the neighborhood of the $5dnd$ (5,3/2), $n=17,19$ perturbers are nicely reproduced. The quasidisappearance of the $5dnd$ (5,5/2) series is simulated by attributing to this channel a large R'_{16} coupling to the open channel and by reducing its excitation matrix element to a level comparable to that of the continuum. Moreover, the channel admixture coefficients in Table I, reveal that the character of this channel is "diluted" to a large number of $5dnd$ $(4,j)$ levels and the (5,3/2) channel, despite the fact that it is not directly coupled to the latter one.

IV. CONCLUSION

We have presented two-step laser photoionization spectra of odd-parity $J=11/2$ autoionizing states of europium atom below the $5d\ ^9D_4$ threshold using the $4f^7 5d6p\ ^{10}F_{9/2}$ inter-

mediate level. The majority of recorded resonances are classified into two $5dnd$ autoionizing Rydberg series converging to the $5d^9D_4$ threshold, observed from $n=15$ to $n=55$, and to two $5dnd$ Rydberg series ($n=13$ to 20) converging to the higher lying $5d\ ^9D_5$ limit. Most of the series exhibit narrow and quasisymmetric line shapes and were measured with an experimental uncertainty of $\sim 0.5\ \mathrm{cm}^{-1}$. The spectra were fitted below as well as above the $5d\ ^9D_3$ limit using appropriate parametric phase-shifted MQDT models. A good overall reproduction was achieved for both level energies and spectral profiles. Furthermore, from the remaining discrepancies the perturbations caused by the single Rydberg series converging to the $5d\ ^9D_3$ threshold as well as three unclassified $J=11/2$ levels (not explicitly taken into account in the MQDT analysis) could be deduced. The former series members were not efficiently excited in the present experiment due to their weak radiative coupling to the intermediate level and/or their large autoionization widths. As for the three unclassified resonances it is speculated that they belong to Rydberg series build on the ^7D_J thresholds. These observations point out the need for further spectroscopic investigations concerning the energy range between the ^9D_J and ^7D_J limits.

The present study is one out of very few applications of MQDT (and the first of phase-shifted MQDT in particular) to lanthanides atoms. Therefore, it is once more demonstrated that this theory may efficiently handle interchannel mixing among Rydberg series even in open shell atoms. Moreover, the level assignments and classification provided by MQDT will be a valuable tool for further understanding and analyzing the structure of the complex europium atom.

[1] M. Aymar, C. H. Greene, and E. Luc-Koening, Rev. Mod. Phys. **68**, 1015 (1996) and references therein.

[2] M. Aymar, A. Debarre, and O. Robaux, J. Phys. B **13**, 1089 (1980); C. B. Xu, X. Y. Xu, W. Huang, M. Xue, and D. Y. Chen, J. Phys. B **27**, 3905 (1994).

[3] S. Bhattacharyya, S. G. Nakhate, T. Jayasekharan, and M. A. N. Razvi, Phys. Rev. A **73**, 062506 (2006).

[4] A. Giusti-Suzor and U. Fano, J. Phys. B **17**, 215 (1984).

[5] W. E. Cooke and C. L. Cromer, Phys. Rev. A **32**, 2725 (1985).

[6] J. M. Lecomte, J. Phys. B **20**, 3645 (1987).

[7] K. Ueda, Phys. Rev. A **35**, 2484 (1987).

[8] A. Giusti-Suzor and H. Lefebvre-Brion, Phys. Rev. A **30**, 3057 (1984).

[9] S. Cohen, Eur. Phys. J. D **4**, 31 (1988).

[10] S. G. Nakhate, M. A. N. Razvi and S. A. Ahmad, J. Phys. B **29**, 1439 (1996).

[11] W. C. Martin, R. Zalubus, and L. Hagan, *Atomic Energy Levels of the Rare Earth Elements*, Natl. Bur. Stand. (U.S.) Circ. No. 60 (U.S. GPO, Washington, D.C., 1978).

[12] S. G. Nakhate, M. A. N. Razvi, J. P. Connerade, and S. A. Ahmad, J. Phys. B **33**, 5191 (2000).

[13] S. Cohen, P. Camus, and A. Bolovinos, J. Phys. B **38**, S1 (2005).

[14] M. A. Baig and S. A. Bhatti, Phys. Rev. A **50**, 2750 (1994).